Enhanced Transverse Strength of 3D Printed Acrylonitrile Butadiene Styrene Parts by Carbon Fiber/Epoxy Pin Insertion

Thang Q. Tran [a,b], Anubhav Sarmah [a], Smita Shivraj Dasari [a], Kailash Arole [c], Matthew J. Cupich [a], Lara A. Amiouny [a], Hang Li Seet [b], Sharon Mui Ling Nai [b], Micah J. Green [a,c,*]

[a] Artie McFerrin Department of Chemical Engineering, Texas A&M University, College Station, TX, 77843, USA

[b] Singapore Institute of Manufacturing Technology (SIMTech), Agency for Science, Technology and Research (A*STAR), 5 Cleantech Loop, #01-01 Cleantech Two Block B, Singapore 636732, Republic of Singapore

[c] Department of Materials Science and Engineering, Texas A&M University, College Station, TX, 77843, USA

*Corresponding author: E-mail: micah.green@tamu.edu (Micah J. Green)

Abstract

Thermoplastic parts fabricated by material extrusion (MEX) 3D printing usually possess weak inter-layer bonding, leading to low mechanical performance in the Z-direction. Here, we develop a simple but effective post-treatment method to improve the Z-strength of MEX-printed acrylonitrile butadiene styrene (ABS) parts. In this method, commercial carbon fiber (CF) tows and epoxy were embedded into internal channels in MEX-printed structures to form high-strength CF/epoxy pins. Due to the mechanical interlock between the CF/epoxy pins and the printed ABS, the Z-strength of the printed parts improved significantly. Specifically, the Z-pinned ABS samples exhibit a strength of up to 71.74 MPa and a Young's modulus of up to 5.93 GPa in the transverse direction, which were 335% and 266% higher than those of the printed neat counterparts, respectively. We find that the mechanical performance of the Z-

pinned samples follows a simple rule of mixtures which is able to capture the Z-dependent mechanical strength and Young's modulus. Also, curved CF/epoxy pins were successfully formed within printed thin-walled curved structures, offering the capability to strengthen MEX printed structures with complex shapes. This work demonstrates that the Z-pin embedding process can be an effective approach to improve the transverse strength of the MEX printed parts for load-bearing structural applications.

Keywords: Material extrusion, Acrylonitrile butadiene styrene, Z-strength, Z-pin, carbon fiber/epoxy

1. Introduction

In recent years, additive manufacturing (AM) technologies, commonly referred to as 3D printing, has drawn tremendous attention from both industry and academia [1, 2]. These advanced technologies possess several advantages compared with conventional manufacturing techniques, offering new capabilities to process materials [1, 3, 4]. Material extrusion (MEX) 3D printing such as fused filament fabrication (FFF) is one of the most widely used AM methods to process thermoplastics because of its simple process, good reliability, and high cost-effectiveness [5, 6]. In this method, a thermoplastic filament is extruded through a heated nozzle to deposit the polymer melt layer-by-layer and build up 3D parts based on CAD models [2, 7]. This sequential layer deposition approach allows FFF to fabricate complex and tailored thermoplastic products with high precision, reduced material waste, short lead time, and high customization [2, 4]. Therefore, FFF has been widely employed in various industrial sectors, including aerospace [8, 9], automotives [10, 11], electronics [12-14], and healthcare [15, 16].

Despite FFF's widespread adoption, parts fabricated by FFF usually possess poor inter-layer bonding, resulting in low mechanical properties in the transverse direction (Z-direction) [5, 17]. It is well documented that bonding between adjacent rasters occurs at temperatures above the glass transition temperature (T_g) of the polymer feedstocks [6, 18]. However, because the newly extruded material cools quickly and the underlying layers are already cooled, the bonding time of adjacent rasters does not achieve sufficient polymer entanglement across the inter-raster interface [6, 7, 18]. Moreover, incomplete coalescence of neighboring rasters results in residual inter-raster voids, further lowering the mechanical performance of the printed structures [5-7, 17]. Therefore, FFF-printed components usually have poor Z-strength compared to those fabricated by traditional manufacturing methods [17]. These disadvantages restrict the practical applications of the FFF-printed parts to conceptual prototyping rather than fully functional end-use products [2].

Over the last decade, several methods have been developed to improve the Z-strength of the FFF-printed parts [19-36]. Polymer feedstocks have been modified with addition of reversibly crosslinked polymers to generate new covalent bonds between inter-layer interfaces [21] or low molecular weight surface-segregating additives (LMW-SuSAs) to improve the entanglement of the polymer chains between the printed layers [26, 27]. The printing process has been modified with ultraviolet (UV) irradiation for in-situ crosslink generation at the layer interfaces during the printing of polymer feedstocks modified with LMW-SuSAs and photoinitiators [28]. The integration of laser heating [23], dielectric barrier discharge heating [31], or modified heating blocks [30] have been used to increase the bond time for interfacial diffusion during the printing process. Additionally, the printing process can be modified with the use of a vibrating motor attached to the printhead to increase bonding pressure between the deposited rasters during the printing process [24]. Post-annealing [22, 25, 29] and microwave heating [32] have been effectively applied to re-heat the deposited filaments and provide sufficient time for polymer diffusion between the adjacent rasters after the printing process.

Z-pinning is a through-thickness reinforcement approach which has been applied to address the weak Z-strength of FFF-printed parts. This method involves the insertion of Z-aligned pins into the printed polymer structures such that the interfaces between adjacent Z-planes are reinforced. The first application of Z-pinning was reported by Duty *et al.* to mainly address the mechanical anisotropy issue of FFF-printed parts [33]. In their study, polylactic acid (PLA) parts with holes aligned in Z-direction were printed, followed by the in-situ extrusion of the same PLA resin into the holes after the printing of every 6 layers to form Z-pins. The Z-pinned PLA parts demonstrated mechanically isotropic performance with comparable strength achieved in x- and z-directions; however, they reported the Z-strength was lower than in conventional FFF due to the considerable void space formed during the Z-pinning process [33].

In another approach, Todoroki *et al.* inserted a high-strength carbon fiber (CF)/nylon bar into a large hole of a printed CF/nylon structure; they then applied resistive heating to the bar to bond

the bar to the printed matrix [35]. Despite the significant improvement in the Z-strength of the printed composite structure, it was difficult to perfectly insert solid bars into the holes with no gaps [35].

To address this issue, the authors published another study where CF/nylon filaments surrounded by epoxy resin were embedded into a large hole in FFF-printed PLA structures; after curing, the insert forms a high-strength CF/nylon/epoxy pin [34]. The Z-strength of the printed parts improved significantly and was improved by increasing the CF volume fraction. Moreover, the epoxy resin fills the gaps between the nylon and the printed PLA matrix [34]. However, because this method requires the printed structure to have large holes for easy insertion of the composite filaments, only structures with large size and simple shapes (such as large tensile coupons or thick walls) were reinforced using this method [34].

In this paper, we aim to enhance the Z-strength of the FFF printed ABS parts by employing a simple but effective post-treatment method. In this method, narrow channels with different shapes were introduced into the internal structure of printed ABS parts, followed by the embedding of commercial CF tows and epoxy. Due to compatibility between the sized CF tow and the epoxy as well as strong mechanical interlock between the composite pins and the printed matrix, high reinforcing efficiency can be achieved, leading to significant improvement in Z-strength of the printed structures after the embedding process. The rule of mixtures can accurately predict the mechanical performance of the Z-pinned samples, allowing the composition of the composite pins to be designed for required loads. Additionally, the flexibility of the CF tows and the used narrow channels allows curved CF/epoxy pins to be formed to strengthen complex printed structures. The results suggest that the Z-pin insertion process can be an effective post-treatment approach to improve the Z-strength of the FFF printed parts for final end-use applications.

2. Materials and Methods

2.1. Materials

ABS filament was purchased from Raise3D Technologies, Inc. (USA). Continuous unidirectional CF tows (T700SC-12K-50C) were obtained from Toray Composite Materials America, Inc. (USA). As shown in **Fig. S1**, the tow consists of 12,000 filaments coated with 1.5 wt.% sizing agent. Epoxy resin (EPON resin 828) was provided by Hexion, Inc. (USA) and curing agent (Jeffamine T403 polyetheramine) was obtained from Huntsman Corporation (USA). Two-part thermosetting epoxy were prepared by mixing the resin and the curing agent at a weight ratio of 100:49 using a planetary mixer (Thinky corporation, AR-100).

2.2. Dimension of ABS tensile samples

Fig. S2 shows the drawings and cross-sections of standard, one-channel and two-channel tensile samples used in this study. The dimension of the standard tensile samples follows ASTM D638 type I with a dimension of 165 mm × 19 mm × 4 mm. An L-shape channel with a cross-section of 1.6×1.6 mm^2 was introduced to the center of the coupons to form one-channel sample. The outlet of the channel has a smaller size (0.5×0.5 mm^2) for easy sealing. A U-shape channel with a cross-section of 1.6×1.6 mm^2 and a channel edge of 3.2 mm were introduced into the tensile coupons to form two-channel samples.

2.3. 3D printing of ABS samples

Tensile specimens and demonstrator parts were printed by using an INTAMSYS FUNMAT HT printer equipped with a 0.4-mm-diameter nozzle. The computer aided design (CAD) models of the specimens were sliced by INTAMSUITE software to generate G-code files for the printing process. The printing parameters of ABS template settings in the INTAMSUITE slicer were used for the printing process as recommended by INTAMSYS manufacturer. Specifically, temperature of nozzle, chamber, and build plate were set at 250 °C, 40 °C, and 90 °C,

respectively. A raft with a thickness of 1.675 mm was printed before the deposition of the main specimens to avoid warpage. All samples were printed at a layer height of 0.25 mm with a shell number of 2 and a printing speed of 60 mm/s. An infill angle of [45°/-45°] and an infill density of 100% were used because it is the most widespread configuration used for FFF printed structures. An infill overlap of 5% was employed to generate good bonding between the shell and the infill. The prints of the standard, one-channel and two-channel tensile samples are presented in **Fig. S3.**

2.4 Volume fraction of each component of the tensile samples

To determine the volume fraction of each component of the tensile samples, the gage length region of the samples and the CF tows with a length of 50 mm were cut and their mass was measured, as shown in **Figs. S4**. Based on the mass differences between the air-pin samples and the others, the amount of epoxy injected into the channels can be determined for volume fraction evaluation.

2.5. Characterization

The width and thickness of all samples were measured by a Vernier caliper at several positions along their length. The mass of the samples was measured by using an analytical balance (XSR204DR, Mettler-Toledo LLC). The cross-sections and fracture surfaces of the tensile samples were characterized by using an optical microscope (BX51, Olympus).

The tensile test of all samples was performed by employing an MTS Insight Electromechanical Testing System equipped with a laser extensometer for high accuracy strain measurements. According to ASTM D638 [17], five specimens for each sample were prepared and tested at an elongation rate of 5 mm/min with a gauge length of 50 mm.

3. Results and discussion

3.1. Z-pin insertion process

The layer configurations of the printed samples are shown in **Figs. 1 a-c**. Notably, the one-channel and two-channel samples had additional shell regions at channels and, therefore, more overlap regions were generated between the infill and the internal shell. **Fig. 1d** presents the Z-pin insertion process to produce CF/epoxy pin samples. After the samples with channels were printed, CF tows were manually inserted and epoxy was injected into the channels. Only one CF tow is inserted into the channel of the one-channel sample to form 1 CF/epoxy pin samples. The two-channel samples required two CF tows for the insertion process and the pinned samples are named as 2 CF/epoxy pin samples. To investigate reinforcing effects of different pin types on the transverse mechanical performance of the printed parts, tensile samples without embedment of any additional component and with only epoxy were also prepared. Since no physical pins were formed in the internal channels, the samples without embedment of any components are named as 1 air pin samples for one-channel sample and 2 air pin samples for two-channel samples. Samples with the injection of only epoxy are named as 1 epoxy pin sample and 2 epoxy pin samples for L-shape samples and U-shape samples, respectively. After the injection of epoxy into the L-shape channels, the outlet of both 1 epoxy pin and 1 CF/epoxy pin samples was sealed by soldering. Finally, the samples were kept standing for more than 24 h to cure the epoxy before mechanical testing.

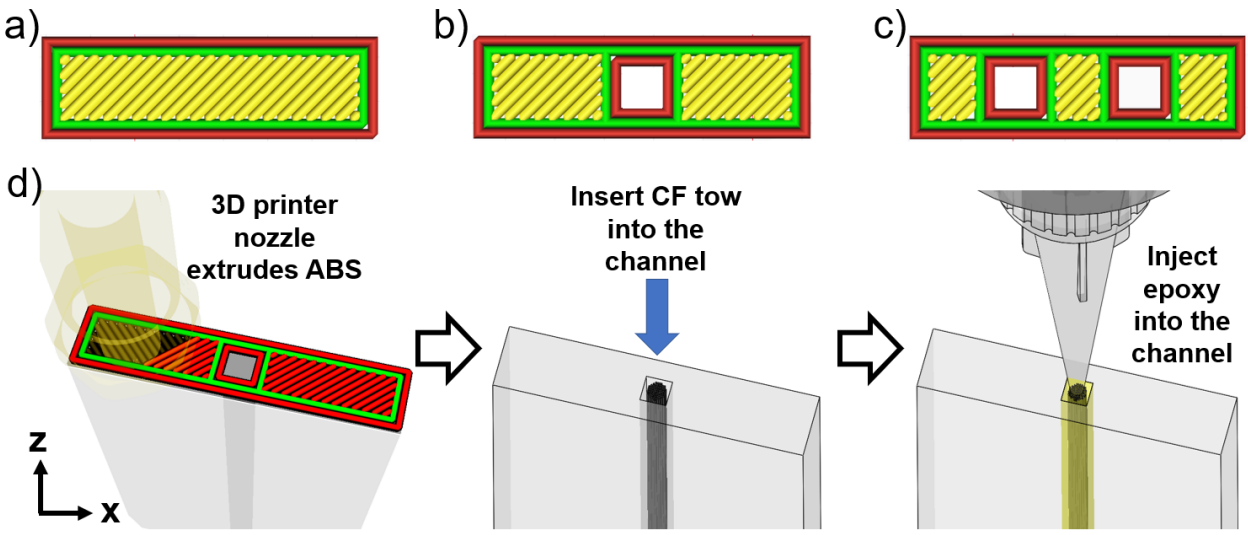

Fig. 1. Printed layer configuration of a) standard sample, b) L-shape channel sample, and c) U-shape channel sample. d) Schematic diagram showing Z-pin insertion process.

3.2. Morphology of the printed ABS samples

Fig. 2 shows the cross-sections of ABS tensile samples with and without Z-pins. Both L-shape and U-shape channels were successfully introduced into the printed ABS tensile samples by modifying the CAD models to form the air pin samples, as shown in **Fig. 2a**. Also, epoxy and CF tows were successfully embedded into the narrow channels to generate epoxy pin and CF/epoxy pin samples. The cross-sections of the samples at the gauge length presented in **Fig. 2b** indicate that there were no visible gaps formed between the pins and the printed ABS matrix. The result suggests that the Z-pin insertion process can form Z-pins with different configurations in the internal structure of the printed ABS samples.

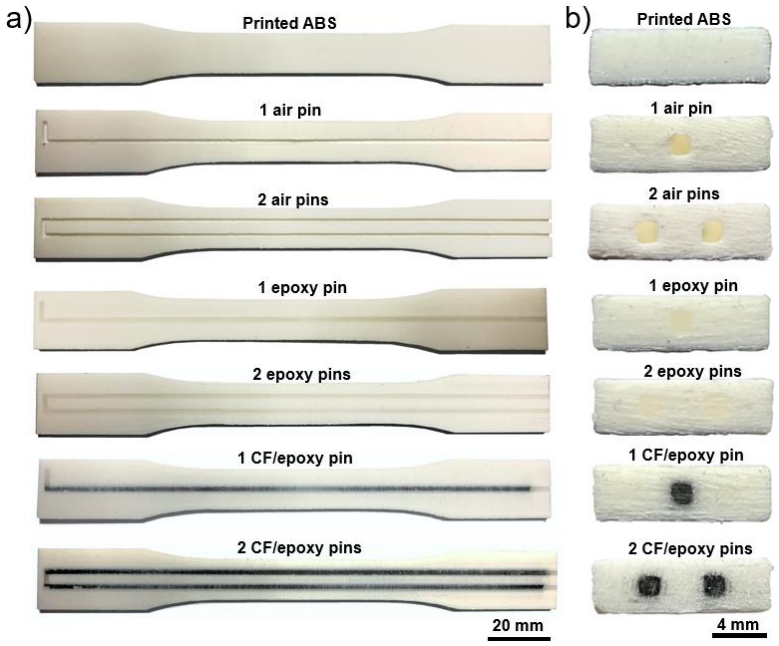

Fig. 2. Cross-sections of the ABS samples in longitudinal direction (a) and in transverse direction at the gauge length position (b).

Fig. 3 presents morphologies of all Z-pins formed by the pin insertion process. Although the channels with rectangular cross-section were included in the CAD models, the corners of the printed channels were rounded because of the fast movement of the printing nozzle (**Fig. 3a**).

Due to the nature of MEX 3D printing process, the surface of the printed parts possesses unique texture formed by deposited rasters (**Figs. 3b and c**). As shown in **Figs. 3d and g**, there were no visible gaps between the epoxy pin or the CF/epoxy pin and the printed ABS matrix. Moreover, both pins possess surface texture similar to that of the printed channels (**Figs. 3e, f, k and h**), suggesting that the low viscosity of the epoxy allows it to easily flow and fill up the narrow channels.

Generally, the texture formed by deposited rasters is undesirable because it lowers the surface quality of the printed parts and, therefore, additional post-processing steps such as polishing are usually required to reduce the surface roughness [37]. However, the rough surface texture of the printed internal channels is highly advantageous for Z-pin insertion process because it can generate better mechanical interlock between the pins and the printed matrix [38]. Since there are no chemical bond between epoxy and ABS matrix, their strong mechanical interlock plays a crucial role on improving reinforcing efficiency of the Z-pins.

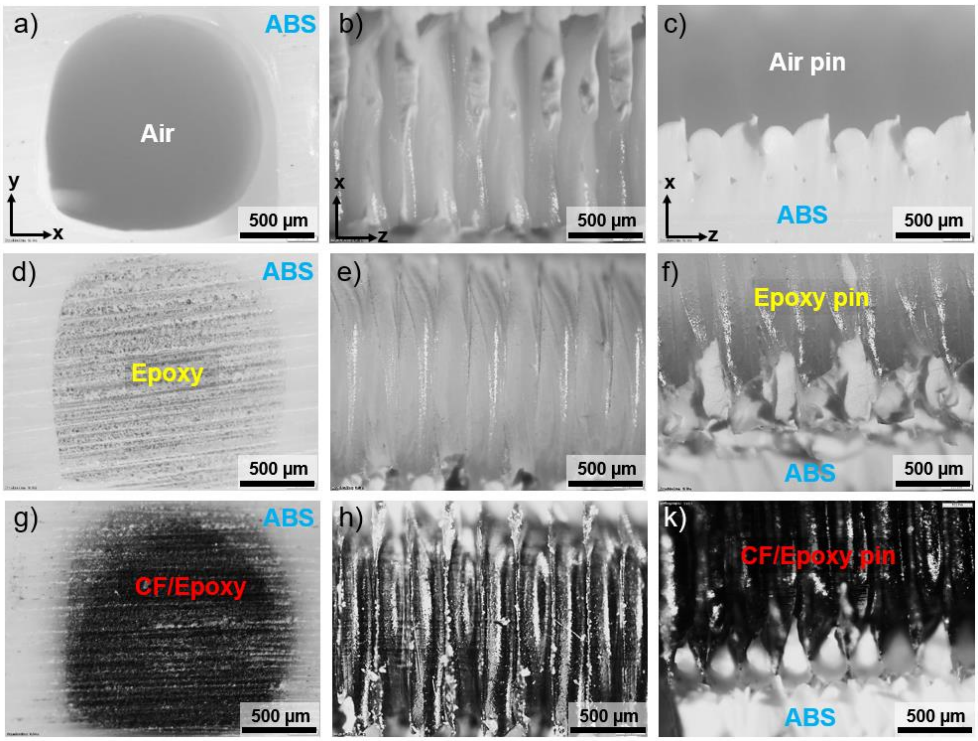

Fig. 3. Optical microscopy images showing morphologies of Z-pins: air pin (a, b, c), epoxy pin (d, e, f), and CF/epoxy pin (g, h, k)

3.3. Mechanical properties of the ABS samples

Fig. 4 presents the stress-strain curves, fractured samples, and the mechanical properties of different tensile samples in Z-direction. All tensile samples broke within the gauge length, indicating that all tensile tests were valid (**Fig. 4b**). The molded epoxy samples possessed a strength of 44.01 MPa and Young's modulus of 2.86 GPa, which is much better than the mechanical properties of the ABS parts printed in longitudinal **(Fig. S5)** and transverse directions. With the addition of L-shape and U-shape channels, the mechanical performance of the air-pin samples was slightly lower than that of the printed ABS counterparts because these channels reduced the amount of load-bearing material.

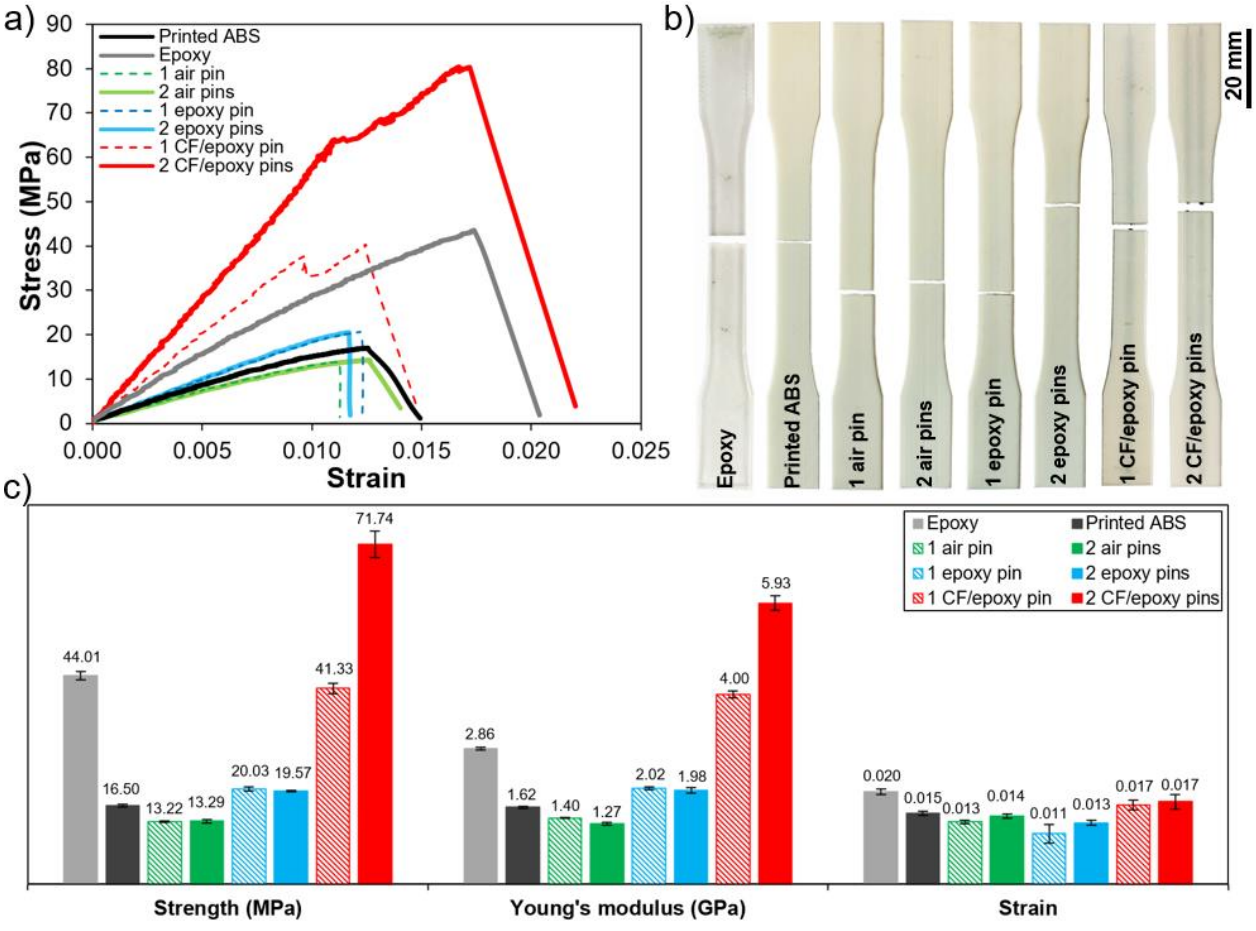

Fig. 4. a) Stress-strain curves of epoxy and ABS tensile samples, b) Fractured tensile samples of epoxy and ABS tensile samples, and c) Mechanical properties of epoxy and ABS tensile samples.

With the strong reinforcement of the epoxy pins, the tensile strength and Young's modulus of the epoxy-pin samples were 21.39% and 24.69% higher than those of the printed ABS samples, respectively. Since the strain at break of the printed ABS (~0.015) was lower than that of the epoxy (~0.02), the printed ABS matrix would break first before the failure of the epoxy pin during the tensile test. However, the epoxy pin could not withstand the high load after the failure of the ABS matrix. Therefore, they broke immediately, resulting in the formation of only one peak in their stress-strain curve of the 1 epoxy pin and 2 epoxy pin samples, as shown in **Fig. 4a**. Notably, the curing process of the epoxy is exothermic with a heat of polymerization is approximately 298 J/g [39]. However, due to the small amount of the epoxy loading and its slow curing speed at room temperature, the released energy at each composite pin during the curing process was very low (~0.004 J/s). Therefore, the heat of polymerization has insignificant effects on the temperature increase of the Z-pinned sample during the curing process and on the final mechanical performance of the samples.

Due to the superior mechanical properties of the CF tows, the integration of the CF/epoxy pins could significantly improve the mechanical performance of the printed ABS samples. Specifically, the 1 CF/epoxy pin samples possessed a tensile strength and Young's modulus of 41.33 MPa and 4.00 GPa, which were 150% and 147% higher than those of the printed ABS counterparts. The addition of another CF/epoxy pin could improve the tensile strength and Young's modulus of the tensile samples by 74% and 48%, reaching 71.74 MPa and 5.93 GPa, respectively. The strain at break of the CF/epoxy samples was also slightly higher than that of the printed ABS, probably due to the higher strain at break of the CF tows. These results are significantly higher than mechanical performance of the Z-pinned PLA samples reported by Kajimoto *et al.* after the samples were reinforced with CF/Nylon/Epoxy pins at similar CF volume fraction [34].

Notably, the fracture behavior of the CF/epoxy pin samples was quite different from the other tensile samples with 2 main peaks observed in their stress-strain curves (**Fig. 4a**). The first peak

was correlated with the early failure of the ABS matrix due to its lowest strain at break compared to epoxy and CF tows. Unlike the epoxy pins, the CF/epoxy composite pins had significantly high strength, and therefore, they could withstand the high load after the failure of the ABS matrix. As the strain increases, the tensile stress continued to increase to form the second peak of the stress-strain curve until the failure of the CF/epoxy pins. Therefore, the ultimate tensile strength of the CF/epoxy pin samples were mainly determined by the mechanical properties of the CF tows used in the insertion process. The results suggest that CF/epoxy pins formed by the Z-pin insertion process can effectively improve the Z-strength of the printed ABS parts.

Fig. 5 shows the fracture surfaces of different tensile samples. A typical fracture surface of the epoxy tensile samples can be observed in **Figs. 5a-c** with three different zones: a flat featureless mirror zone around the crack initiation point, a transition zone with gradual increase of surface roughness, and a final propagation zone with conical marks [40]. **Figs. 5d-f** present a typical fracture surface of the printed ABS samples in transverse direction. Under tensile load application, crack mainly propagated within one inter-layer interface due to the weak inter-layer bonding of the printed structure [17]. Several inter-raster voids were observed within the infill region (**Fig. 5e**), whereas denser regions were found at overlap regions between the infill and the shell due to the 5% infill overlap setting [6, 7]. Similar to the fracture surface of the printed ABS samples, the fracture surface of the 1-air-pin samples also possessed several inter-raster voids because of the large infill region in the printed structure (**Fig. 5h**) The cross-section of the air pin could also be observed in **Fig. 5i**. Compared to the 1-air-pin samples, the 2-air-pin samples possessed more dense regions and less inter-raster voids due to more overlap regions around the two air pins (**Fig. 5k**). This explains the comparable mechanical performance of the 1-air-pin and 2-air-pin samples although the 2-air-pin samples possessed higher pin number.

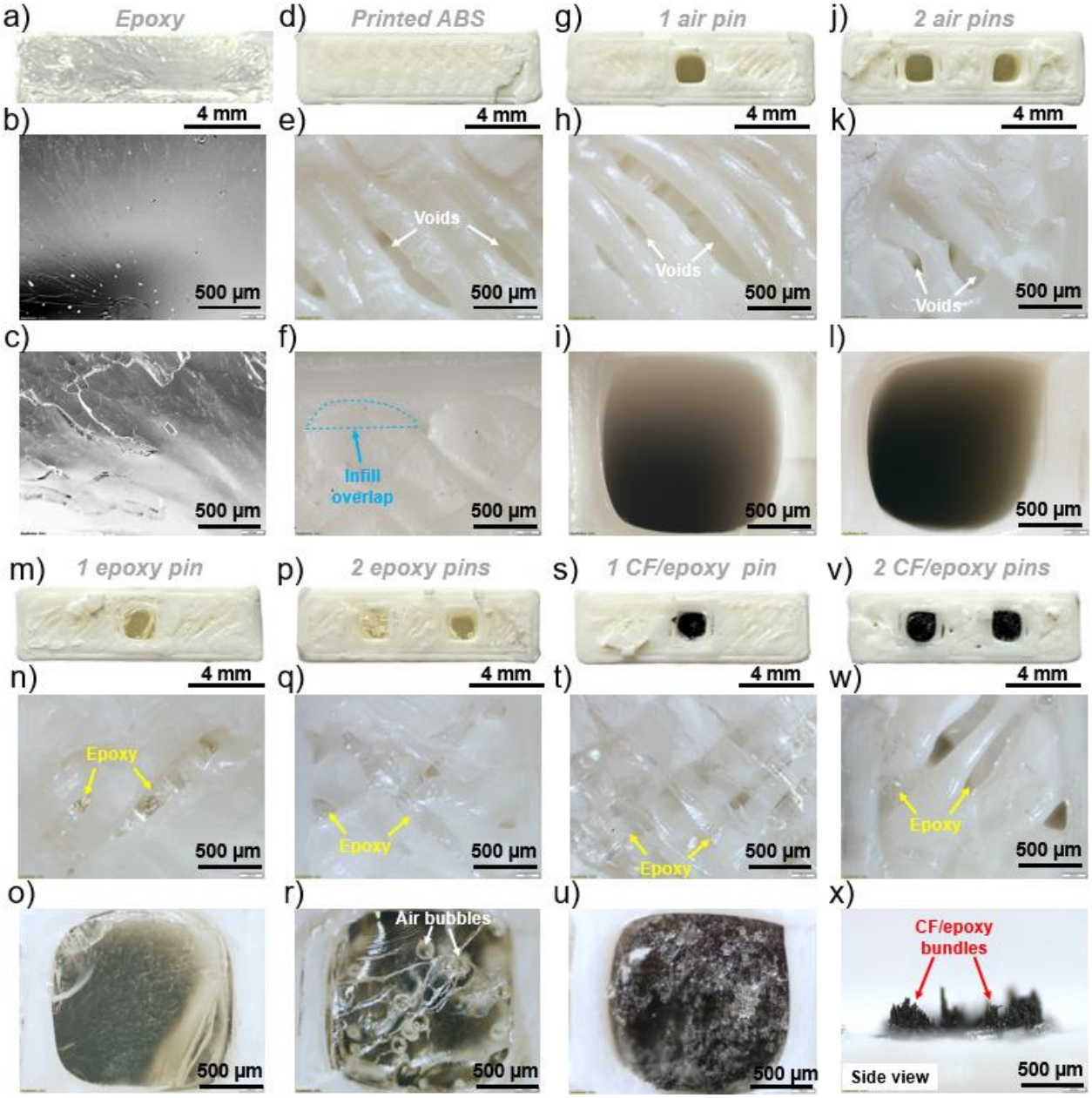

Fig. 5. Fracture surfaces of different tensile samples at different magnifications: (a, b, c) molded epoxy samples; (d, e, f) printed ABS samples; (g, h, i) 1 air pin samples; (j, k, l) 2 air pin samples; (m, n, o) 1 epoxy pin samples ; (p, q, r) 2 epoxy pin samples ; (s, t, u) 1 CF/epoxy samples ; (v, w, x) 2 CF/epoxy pin samples

Figs. 5m-r present the fracture surfaces of the epoxy-pin samples. Epoxy was observed in the voids and gaps between the deposited ABS rasters, suggesting that the epoxy flowed into the printed ABS structures and partly filled up the inter-raster voids during the Z-pin insertion process (**Figs. 5n and q**). Interestingly, typical features of fractured epoxy can be observed in

the pin fracture surface of the 1-epoxy-pin samples (**Fig. 5o)** and several air bubbles were found at the pin fracture surface and inside the pin structure of the 2-epoxy-pin samples (**Fig. 5r**).

Figs. 5s-x show the fracture surfaces of the CF/epoxy-pin samples. More epoxy was found at their fracture surface compared to that of the epoxy-pin samples (**Figs. 5t and w**). Because the channels were mainly occupied by the CF tows during the Z-pin insertion process, high pressure was required to inject epoxy into the channels, resulting in better infiltration of the epoxy into the internal structure of the printed ABS matrix. More importantly, the pull-out length of the fractured CF tows and the epoxy at the fracture surface shown in **Fig. 5x** was very short (~300 μm). This pull-out length is much shorter than the that of the composite filaments used to reinforce the Z-strength of printed PLA structure reported by Kajimoto *et al.* [34]. The results suggest that the Z-pin insertion method can provide strong interfacial bonding and high stress transfer efficiency between the CF/epoxy pins and the printed ABS matrix.

3.4. Comparison against rule of mixtures

Based on the mass of the gauge length region of the samples shown in **Fig. S6**, volume fraction of different components of the tensile sample was determined and presented in **Table 1**. As aforementioned, the printed ABS structures possessed many inter-raster voids. After the Z-pin insertion process, the volume fraction of the printed ABS component in the samples slightly reduced because the injected epoxy partly filled up the internal voids of the printed ABS structures, as observed in **Fig. 6**.

Table 1. Volume fraction of different components in the gauge length region of the tensile samples.

Components	1 air pin	2 air pins	1 epoxy pin	2 epoxy pins	1 CF/epoxy pin	2 CF/epoxy pins
Printed ABS	95.1	90.2	89.7	85.9	86.0	80.5
Epoxy	0.0	0.0	10.3	14.1	13.1	17.7
CF	0.0	0.0	0.0	0.0	0.9	1.8

The general rule of mixtures provides a weighted average for mechanical properties such as Young's modulus and even non-linear properties such as tensile strength [34, 41]. For Young's modulus, the equation is written as

$$E_{total} = V_{f\_ABS}E_{ABS} + V_{f\_Epoxy}E_{Epoxy} + V_{f\_CF}E_{CF} \quad (1)$$

where E_{total} represents the estimated value of Young's modulus. V_{f_ABS}, V_{f_Epoxy}, and V_{f_CF} are volume fraction of printed ABS, epoxy, and carbon fiber, respectively. E_{ABS}, E_{Epoxy}, and E_{CF} are Young's modulus of printed ABS, epoxy, and carbon fiber, respectively. The volume fractions of the components in our system are summarized in **Table 1**.

The rule of mixtures for tensile strength is more complex. In some cases (case I), only the strongest component is considered because that component breaks the last. In the other cases (case II), two components break together and the observed strength is an average of the tow. Experimental data is needed to know which case is more relevant [41]. Based on the fracture behavior of the composites shown in Section 3.3, the rule of mixtures can be applied to determine the estimated value of their tensile strength by using equation (2-4).

For the air-pin samples (case I): $\sigma_{Air\ pin} = V_{f\_ABS}\sigma_{ABS}$ (2)

For the epoxy-pin samples (case II): $\sigma_{Epoxy\ pin} = V_{f\_ABS}\sigma_{ABS} + V_{f\_Epoxy}\sigma'_{Epoxy}$ (3)

For CF/epoxy-pin samples (case I): $\sigma_{CF/Epoxy\ pin} = V_{f\_CF}\sigma_{CF}$ (4)

where $\sigma_{Air\ pin}$, $\sigma_{Epoxy\ pin}$, and $\sigma_{CF/epoxy\ pin}$ are estimated values of tensile strength of air-pin, epoxy-pin, and CF/epoxy-pin samples. σ_{ABS} and σ_{CF} are tensile strength of printed ABS and carbon fiber, respectively. σ'_{Epoxy} is the tensile strength of epoxy at the strain to failure of printed ABS matrix (0.015) [34].

Table 2. Strength and Young's modulus of printed ABS, epoxy, and CF filament.

	Printed ABS	**Epoxy**	**CF filament**
Strength (MPa)	16.51	40.68	4900

Young's modulus (GPa)	1.62	2.86	230

Table 2 shows the strength and Young's modulus of ABS, epoxy, and CF filament used to determine estimated strength and Young's modulus of the tensile samples. The strength and Young's modulus of the printed ABS and epoxy were obtained from experimental measurements shown in Section 3.3, whereas the values for CF filaments were obtained from their manufacturer. The tensile strength of epoxy used for the evaluation was the stress of the epoxy at the strain to failure of the ABS matrix (0.015).

Fig. 6 compares the experimental strength and Young's modulus and the estimated values obtained from the rule of mixtures. The experimental strength and Young's modulus of the air-pin samples were slightly lower than the rule of mixtures estimates probably due to effects of different layer configurations used for the printing of ABS structures. The experimental data of the epoxy-pin samples were slightly higher than the rule of mixtures because not only the epoxy pins but also the epoxy that filled up the inter-raster voids of the printed ABS structures helped to strengthen the tensile samples further.

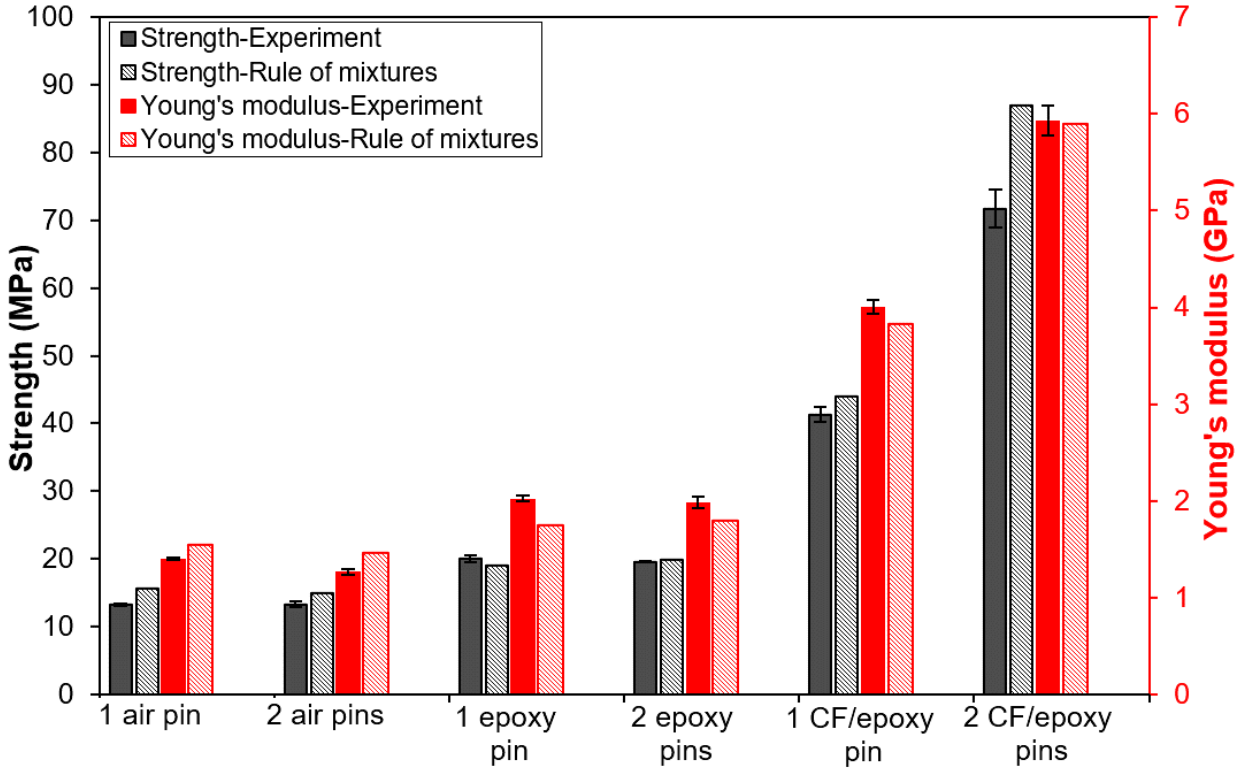

Fig. 6. Comparison between the experimental strength and Young's modulus of the ABS samples and the estimated strength and Young's modulus obtained by the rule of mixtures.

For the 1-CF/epoxy-pin samples, their estimated and experimental values are comparable, suggesting that misalignment of CF filaments within the CF tows had insignificant effects on the mechanical performance of the tensile samples. Although comparable values were obtained for the experimental and estimated Young's modulus of the 2-CF/epoxy-pin samples, the experimental strength of the samples is slightly lower than the estimated value. This can be explained by the possible misalignment between the CF/epoxy tows of different composite pins under tensile load [41], especially when the distance between the two pins was 3.2 mm. Therefore, all CF filaments within the 2-CF/epoxy-pin samples might not withstand the tensile load at the same time, leading to their non-uniform fractures and, therefore, lowering their tensile strength. The results suggest that the rule of mixtures can be applied to estimate the mechanical performance of the Z-pinned samples as well as to determine the number and configurations of Z-pinned structures to meet required mechanical properties for load-bearing applications. Moreover, the uniformity of the channels' cross-section would not affect much on the mechanical properties of the Z-pinned structures because their mechanical performance mainly depends on the volume fraction of the high-strength CF tows.

3.5. Performance comparison

Fig. 7 and **Table S1** compares the tensile strength, Young's modulus, and the improvement percentages of FFF-printed polymer parts produced by our Z-pin insertion process and different other methods [19-32, 34]. Most of the research work focused on improving the interlayer adhesion of the printed structures to enhance their Z-strength. However, the Z-pin insertion methods reported by this work and Kajimoto *et al.* could achieve much better mechanical performance and improvement percentage due to the outstanding reinforcement effect of the continuous fiber reinforced composite pins [34]. More importantly, the volume fraction of the

reinforcing fibers of the Z-pins in these methods can be increased to improve the mechanical performance for desired load-bearing applications. For example, a tensile strength of more than 100 MPa and a Young's modulus of more than 7 GPa were achieved when the volume fraction of carbon fiber of the Z-pin reached 6.4% [34]. Notably, compared to the Z-pin insertion method reported by Kajimoto *et al.,* our method has much better improvement percentage for both tensile strength and Young's modulus at similar volume fraction. This result might be due to the fact that our technique can generate stronger mechanical interlock between the inserted Z-pins and the printed ABS matrix, whereas good compatibility between the epoxy and the sized CF tows can provide better reinforcing effects. Additionally, the different type of CF tows used in our study might also contribute to the better performance of the Z-pinned samples.

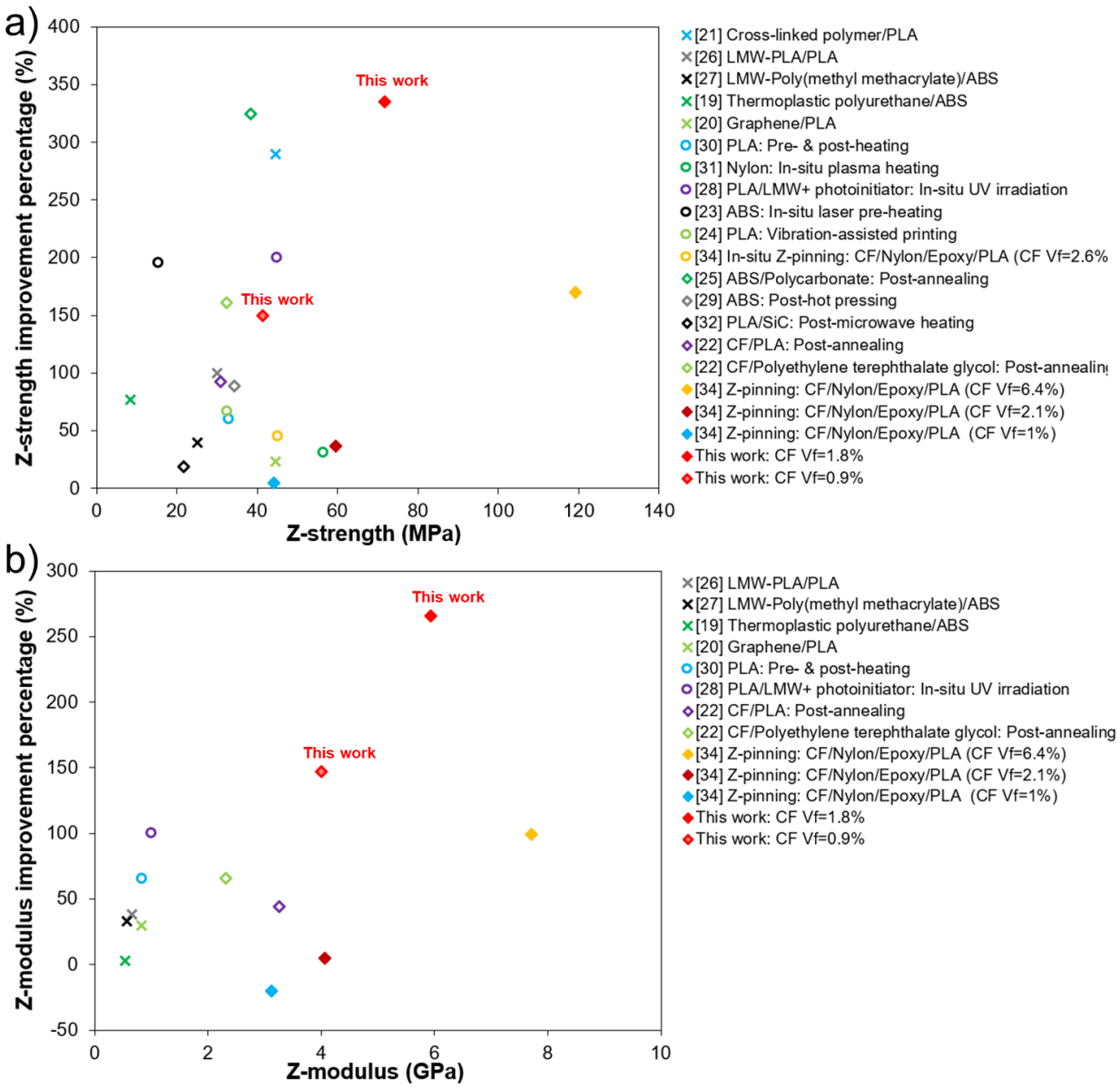

Fig. 7. (a) Tensile strength and strength improvement and b) Young's modulus and Young's modulus improvement of FFF printed polymer parts produced by different methods based on feedstock modification (crosses), process modification (unfilled circles), and post-treatment (filled and unfilled diamonds), and Z-pinning work (filled diamonds).

Compared to conventional methods using rigid rods as Z-pins, our method can produce not only the straight but also the curved composite pins with controlled compositions and sizes to strengthen FFF-printed structures due to the use of CF tows. This offers unique capability to reinforce complex printed structures which are the crucial advantages of AM technologies. To

demonstrate this advantage, 4 curved CF/epoxy pins were embedded into internal structure of a printed hanging vase (**Figs. 8a and b**) and a printed duct adaptor using the L-channel concept (**Figs. 8c and d**). For actual printed components, the Z-pin insertion process can only be applied to regions that are large enough to integrate Z-channels into their internal structures. Because the 12K CF tows were used to fabricate Z-pins in this study, the printed parts needed to have a thickness of at least 4 mm to allow the Z-channel generation. However, the minimum required size of the printed structures for the insertion process can be reduced significantly by using smaller CF tows such as 1K tows to fabricate smaller Z-pins. This approach can broaden the applications of the Z-pin insertion process to parts with more complex shapes and various sizes.

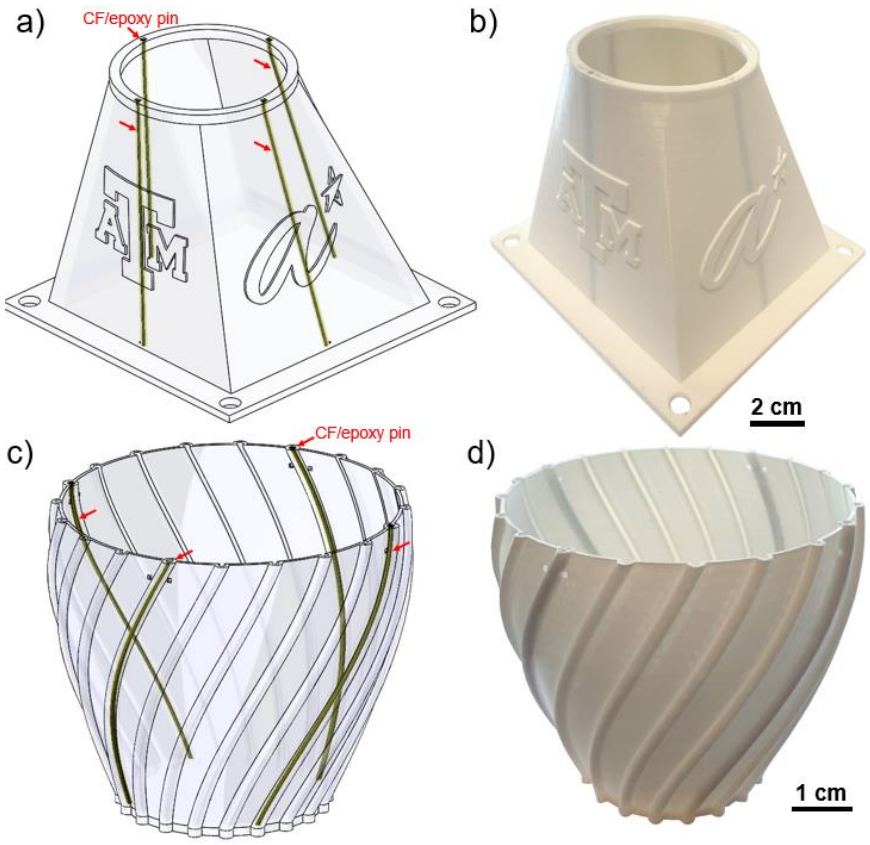

Fig. 8. Complex printed structures reinforced with molded Z-pins: CAD model (a) and printed part (b) of a duct adapter reinforced with molded Z-pins; CAD model (c) and printed part (d) of a hanging pot reinforced with molded Z-pin.

4. Conclusion

In summary, an effective post-treatment method was successfully developed to improve the mechanical performance of FFF printed ABS parts in the Z-direction. In this method, high-strength CF/epoxy pins were formed in internal channels of FFF printed ABS structure by embedding commercial carbon fiber tows and epoxy. Because of the good compatibility between the CF tows and the epoxy as well as the strong mechanical interlock formed between the composite pins and the printed ABS matrix, good mechanical reinforcement can be achieved in the Z-direction, leading to an improvement of up to 335% in tensile strength and 266% in Young's modulus. Moreover, composition of the Z-pinned samples can be tailored based on rule of mixture to achieve desired mechanical performance. More importantly, the flexibility of the CF tows allows the Z-pin insertion method to fabricate curved CF/epoxy pins for strengthening complex FFF printed structures. The results indicate that the Z-pin insertion process has the potential to mechanically reinforce the FFF printed parts in the Z-direction for end-use applications. In the future, the automation and integration of the process into printer hardware will be investigated. Additionally, localized heating methods based on radio frequency, infrared radiation, and dielectric barrier discharge will be combined with the Z-pin insertion method to improve the Z-strength of the Z-pinned structures further while reducing the curing time and the energy consumption of the epoxy curing process.

CRediT authorship contribution statement

Thang Q. Tran: Conceptualization, Methodology, Investigation, Writing – original draft, review & editing. **Anubhav Sarmah**: Investigation. **Smita Dasari**: Investigation. **Kailash Arole**: Investigation. **Matthew J. Cupich**: Investigation. **Lara A. Amiouny**: Investigation. **Hang Li Seet**: Writing – review & editing. **Sharon Mui Ling Nai**: Writing – review & editing. **Micah J. Green**: Conceptualization, Writing – review & editing.

Declaration of competing interest

The authors declare that they have no known competing financial interests or personal relationships that could have appeared to influence the work reported in this paper.

Acknowledgments

The authors acknowledge A*STAR Graduate Academy - A*STAR International Fellowship Program for their sponsorship. Use of the Texas A&M University Soft Matter Facility (RRID:SCR_022482) for TGA is acknowledged. The authors thank the Materials and Testing Lab at TAMU for their Mechanical Testing setup.

Appendix A. Supporting information

References

[1] A.G. Crowley, T.Q. Tran, M.J. Green, Using nanomaterials to enhance the additive manufacturing of polymeric resins, Nano Futures 6 (2022) 042502.

[2] T.Q. Tran, F.L. Ng, J.T.Y. Kai, S. Feih, M.L.S. Nai, Tensile Strength Enhancement of Fused Filament Fabrication Printed Parts: A Review of Process Improvement Approaches and Respective Impact, Additive Manufacturing 54 (2022) 102724.

[3] A. Sarmah, R.D. Mee, K. Arole, D. Chi, E.M. Harkin, S.S. Dasari, A.J.K. Wright, T.Q. Tran, A. Rout, M.J. Green, Competing Effects of Radio Frequency Fields on Carbon Nanotube/Resin Systems: Alignment versus Heating, Macromolecular Materials and Engineering (2023) 2300174.

[4] X. Zhou, L. Wu, J. Wang, Recent developments in conductive polymer composites for fused deposition modeling, Composites Part A: Applied Science and Manufacturing 174 (2023) 107739.

[5] X. Sun, M. Mazur, C.-T. Cheng, A review of void reduction strategies in material extrusion-based additive manufacturing, Additive Manufacturing 67 (2023) 103463.

[6] T.Q. Tran, X. Deng, C. Canturri, C.L. Tham, F.L. Ng, Highly-dense acrylonitrile butadiene styrene specimens fabricated by overheat material extrusion 3D printing, Rapid Prototyping Journal 29 (2023) 687-696.

[7] T.Q. Tran, C. Canturri, X. Deng, C.L. Tham, F.L. Ng, Enhanced tensile strength of acrylonitrile butadiene styrene composite specimens fabricated by overheat fused filament fabrication printing, Composites Part B: Engineering 235 (2022) 109783.

[8] Y. Abderrafai, A. Diouf-Lewis, F. Sosa-Rey, R.D. Farahani, N. Piccirelli, M. Lévesque, D. Therriault, Additive manufacturing and characterization of high temperature thermoplastic blends for potential aerospace applications, Composites Science and Technology 231 (2023) 109839.

[9] J. Pierre, F. Iervolino, R.D. Farahani, N. Piccirelli, M. Lévesque, D. Therriault, Material extrusion additive manufacturing of multifunctional sandwich panels with load-bearing and acoustic capabilities for aerospace applications, Additive Manufacturing 61 (2023) 103344.

[10] P. Cheng, Y. Peng, S. Li, Y. Rao, A. Le Duigou, K. Wang, S. Ahzi, 3D printed continuous fiber reinforced composite lightweight structures: A review and outlook, Composites Part B: Engineering 250 (2023) 110450.

[11] M. Wiese, S. Thiede, C. Herrmann, Rapid manufacturing of automotive polymer series parts: A systematic review of processes, materials and challenges, Additive Manufacturing 36 (2020) 101582.

[12] T.Q. Tran, A. Sarmah, E.M. Harkin, S.S. Dasari, K. Arole, M.J. Cupich, A.J.K. Wright, H.L. Seet, S.M.L. Nai, M.J. Green, Radio frequency-assisted curing of on-chip printed CNT/silicone heatsinks produced by material extrusion 3D printing, Additive Manufacturing 78 (2023) 103842.

[13] D. Xiang, X. Zhang, E. Harkin-Jones, W. Zhu, Z. Zhou, Y. Shen, Y. Li, C. Zhao, P. Wang, Synergistic effects of hybrid conductive nanofillers on the performance of 3D printed highly

elastic strain sensors, Composites Part A: Applied Science and Manufacturing 129 (2020) 105730.

[14] C.J.C. Nocheseda, L.I.M. Ballesteros, M.L.M.L. Grande, E.B. Caldona, R.C. Advincula, Copper-nickel electroplating of 3D-printed acrylonitrile butadiene styrene for interference and radiation shielding applications, Materials Chemistry and Physics 308 (2023) 128193.

[15] S. Qi, H. Yao, J. Fu, Y. Xie, Y. Li, R. Tian, M. Yu, H. Guo, Magneto-active soft matter with reprogrammable shape-morphing and self-sensing capabilities, Composites Science and Technology 230 (2022) 109789.

[16] B.M. Gackowski, G.D. Goh, M. Sharma, S. Idapalapati, Additive manufacturing of nylon composites with embedded multi-material piezoresistive strain sensors for structural health monitoring, Composites Part B: Engineering 261 (2023) 110796.

[17] F.L. Ng, T.Q. Tran, T. Liu, A methodology to develop part acceptance criteria model using non-destructive inspection technique for FDM printed part, Materials Today: Proceedings 70 (2022) 310-316.

[18] X. Gao, S. Qi, X. Kuang, Y. Su, J. Li, D. Wang, Fused filament fabrication of polymer materials: A review of interlayer bond, Additive Manufacturing 37 (2021) 101658.

[19] A.S. de León, A. Domínguez-Calvo, S.I. Molina, Materials with enhanced adhesive properties based on acrylonitrile-butadiene-styrene (ABS)/thermoplastic polyurethane (TPU) blends for fused filament fabrication (FFF), Materials & Design 182 (2019) 108044.

[20] S. Rostom, M.D. Dadmun, Improving heat transfer in fused deposition modeling with graphene enhances inter filament bonding, Polymer Chemistry 10 (2019) 5967-5978.

[21] G.A. Appuhamillage, J.C. Reagan, S. Khorsandi, J.R. Davidson, W. Voit, R.A. Smaldone, 3D printed remendable polylactic acid blends with uniform mechanical strength enabled by a dynamic Diels–Alder reaction, Polymer Chemistry 8 (2017) 2087-2092.

[22] S. Bhandari, R.A. Lopez-Anido, D.J. Gardner, Enhancing the interlayer tensile strength of 3D printed short carbon fiber reinforced PETG and PLA composites via annealing, Additive Manufacturing 30 (2019) 100922.

[23] J. Du, Z. Wei, X. Wang, J. Wang, Z. Chen, An improved fused deposition modeling process for forming large-size thin-walled parts, Journal of Materials Processing Technology 234 (2016) 332-341.

[24] S. Jiang, Y. Siyajeu, Y. Shi, S. Zhu, H. Li, Improving the forming quality of fused filament fabrication parts by applied vibration, Rapid Prototyping Journal 26 (2020) 202-212.

[25] B. Koker, R. Ruckdashel, H. Abajorga, N. Curcuru, M. Pugatch, R. Dunn, D.O. Kazmer, E.D. Wetzel, J.H. Park, Enhanced interlayer strength and thermal stability via dual material filament for material extrusion additive manufacturing, Additive Manufacturing 55 (2022) 102807.

[26] N.P. Levenhagen, M.D. Dadmun, Interlayer diffusion of surface segregating additives to improve the isotropy of fused deposition modeling products, Polymer 152 (2018) 35-41.

[27] N.P. Levenhagen, M.D. Dadmun, Improving Interlayer Adhesion in 3D Printing with Surface Segregating Additives: Improving the Isotropy of Acrylonitrile–Butadiene–Styrene Parts, ACS Applied Polymer Materials 1 (2019) 876-884.

[28] N.P. Levenhagen, M.D. Dadmun, Reactive Processing in Extrusion-Based 3D Printing to Improve Isotropy and Mechanical Properties, Macromolecules 52 (2019) 6495-6501.

[29] R. Rane, A. Kulkarni, H. Prajapati, R. Taylor, A. Jain, V. Chen, Post-Process Effects of Isothermal Annealing and Initially Applied Static Uniaxial Loading on the Ultimate Tensile Strength of Fused Filament Fabrication Parts, Materials 13 (2020) 352.

[30] D. Ravoori, H. Prajapati, V. Talluru, A. Adnan, A. Jain, Nozzle-integrated pre-deposition and post-deposition heating of previously deposited layers in polymer extrusion based additive manufacturing, Additive Manufacturing 28 (2019) 719-726.

[31] C.B. Sweeney, M.L. Burnette, M.J. Pospisil, S.A. Shah, M. Anas, B.R. Teipel, B.S. Zahner, D. Staack, M.J. Green, Dielectric Barrier Discharge Applicator for Heating Carbon Nanotube-Loaded Interfaces and Enhancing 3D-Printed Bond Strength, Nano Letters 20 (2020) 2310-2315.

[32] Y. Wang, Z. Liu, H. Gu, C. Cui, J. Hao, Improved mechanical properties of 3D-printed SiC/PLA composite parts by microwave heating, Journal of Materials Research 34 (2019) 3412-3419.

[33] C. Duty, J. Failla, S. Kim, T. Smith, J. Lindahl, V. Kunc, Z-Pinning approach for 3D printing mechanically isotropic materials, Additive Manufacturing 27 (2019) 175-184.

[34] J. Kajimoto, J. Koyanagi, Y. Maruyama, H. Kajita, R. Matsuzaki, Automated interlaminar reinforcement with thickness directional fiber arrangement for 3D printing, Composite Structures 286 (2022) 115321.

[35] A. Todoroki, T. Oasada, M. Ueda, R. Matsuzaki, Y. Hirano, Reinforcing in the lay-up direction with self-heating for carbon fiber composites fabricated using a fused filament fabrication 3D printer, Composite Structures 266 (2021) 113815.

[36] C.B. Sweeney, B.A. Lackey, M.J. Pospisil, T.C. Achee, V.K. Hicks, A.G. Moran, B.R. Teipel, M.A. Saed, M.J. Green, Welding of 3D-printed carbon nanotube–polymer composites by locally induced microwave heating, Science Advances 3 e1700262.

[37] A. Mathew, S.R. Kishore, A.T. Tomy, M. Sugavaneswaran, S.G. Scholz, A. Elkaseer, V.H. Wilson, A. John Rajan, Vapour polishing of fused deposition modelling (FDM) parts: a critical review of different techniques, and subsequent surface finish and mechanical properties of the post-processed 3D-printed parts, Progress in Additive Manufacturing (2023).

[38] J.P.B. van Dam, S.T. Abrahami, A. Yilmaz, Y. Gonzalez-Garcia, H. Terryn, J.M.C. Mol, Effect of surface roughness and chemistry on the adhesion and durability of a steel-epoxy adhesive interface, International Journal of Adhesion and Adhesives 96 (2020) 102450.

[39] L.Q. Liu, H.D. Wagner, A comparison of the mechanical strength and stiffness of MWNT-PMMA and MWNT-epoxy nanocomposites, Composite Interfaces 14 (2007) 285-297.

[40] R. Zhao, W. Luo, Fracture surface analysis on nano-SiO2/epoxy composite, Materials Science and Engineering: A 483-484 (2008) 313-315.

[41] D. Hull, T.W. Clyne, An Introduction to Composite Materials, 2 ed., Cambridge University Press, Cambridge, 1996.

[42] Y.J. You, J.J. Kim, K.T. Park, D.W. Seo, T.H. Lee, Modification of Rule of Mixtures for Tensile Strength Estimation of Circular GFRP Rebars, Polymers 9 (2017) 682.